

Full Paper

Stability analysis of geotechnical properties of slopes by seismic waves

Muhammad Taquiuddin Zakaria, Nordiana Mohd Muztaza*, Muhammad Rabie Omar and Norshidah Yunus

School of Physics, Universiti Sains Malaysia, 11800 Penang, Malaysia

* Corresponding author e-mail: mmnordiana@usm.my

Received: 31 December 2021 / Accepted: 7 July 2022 / Published: 11 July 2022

Abstract: Inherently, the mechanical properties of soil determine the stability of a slope. These vital properties require serious scrutiny since slope instability can lead to a hazardous phenomenon. Geophysical approaches are recognised to give a detailed characterisation of slope stability. However, these approaches are only capable of providing limited information about the dynamic property of soil. Thus, this study assesses the heterogeneity of soil profile using P- and S- wave velocity for the different types of slope conditions. Distinctively, this study emphasises the elastic moduli and soil competence for stability measurement for Universiti Sains Malaysia and Lojing areas. It is well understood that the velocity profiles successfully delineate the subsurface material. A zonation map was produced and reveals that the Universiti Sains Malaysia area provides a more stable zone based on various geotechnical parameters. These parameters include the shear modulus, G_0 ; Young modulus, E ; Poisson's ratio, ν ; material index, M_i ; stress ratio, S_i ; concentration index, C_i ; and density gradient, D_i . We conclude that the Universiti Sains Malaysia area exhibits more competent soil deposits compared to the Lojing area. The values of geophysical and geotechnical parameters provide the preliminary data on defining the competency of the soil, besides reducing the uncertainty of the ground model.

Keywords: seismic refraction, multichannel analysis surface waves, geophysics, geotechnics, environmental geoscience, soil dynamic

INTRODUCTION

Heterogeneity in the topsoil profile plays a detrimental role in widespread severe damages and causes foundation failure [1]. These phenomena result from the lack of subsurface geological information caused by structural features or horizontal variation in stratification [2]. Crucially,

understanding the behaviours of the subsurface requires a collection of comprehensive geological information. This must also include the site characterisation since it necessitates the understanding of soil materials and conditions. Generally, soil response to ground motions has become the basis of site characterisation. For instance, seismic events which promote liquefaction and landslide could pose a significant threat to the stability of the structure. Therefore, increasing the capacity of risk assessment and prediction by employing different mitigation methods helps to reduce the severity of the hazard [3].

In the past decades, slope stability assessments have led to the development of numerous modelling methods. These methods involve predicting slope response to various triggers and evaluating slope deformation. The investigation of subsurface landslide features is necessary to provide preliminary input for forward modelling and subsequent predictions of potential failure events [4]. However, such models still require access to detailed information on geological, mechanical and hydrogeological properties as well as boundary conditions. The application of seismic methods can also provide information on subsurface characteristics and lithology. Essentially, the seismic velocity is dependent on the elasticity and density of the material through which the energy passes. Therefore, the seismic velocity can potentially provide information about the material strength and rock quality [5]. Seismic refraction involves the estimation of P-wave velocity (V_p) of the earth's near-surface material. It has been used to investigate landslides since the early 1960s. The depths estimation of the failure and the lateral extent of the landslide requires a refraction survey [6]. The method relies on the differences in physical properties of the sliding materials and the underlying undisturbed sediment or bedrock that result in different seismic velocities [7]. Multi-channel analysis of surface waves (MASW) is a non-invasive method of estimating the shear-wave velocity (V_s) profile from surface wave energy. The technique gained popularity in the geotechnical and engineering geological fields [8] as well as various shallow geophysical soundings [9]. The most common use of the surface wave's dispersive properties is to obtain the V_s profiles. Generally, the surface wave's dispersive properties produce V_s profiles by analysis of plane waves. An inversion technique retrieves the information measured from surface wave dispersion, which is the phase velocity change across frequencies. With decreasing frequencies, the wave propagates to deeper layers with high velocity due to increasing wavelengths [10]. In the present study, seismic refraction and MASW were employed to assess site characteristics for Universiti Sains Malaysia (USM) and Lojing areas. Here, the derivation of elastic moduli and the competence scale based on the velocity information is also presented. The outcome highlights the advantages of considering the geophysical parameters and deriving geotechnical parameters for defining the competency of the subsurface. This study provides insights into adopting spatial distributions of geophysical and geotechnical properties to minimise the uncertainty in the ground models, with validation from the soil test.

MATERIALS AND METHODS

Study Area and Geology

This study focuses on the stable and the critical slopes, i.e. USM and Lojing areas respectively. A stable slope is a slope with no active modifications. On the other hand, a critical slope is a slope with existing soil movements that exhibit instability. The USM study area is in Penang district, and the geomorphology consists of terrain topography with hills and plains (Figure 1d). Penang is considered granitic due to the substantial underlying igneous rocks. On this basis the

granitic region in Penang can be divided into the northern Penang Pluton and southern Penang Pluton. Essentially, the northern Penang is divided into Feringgi Granite, Tanjung Bungah Granite and Mukah Head Granite (microgranite) [11]. The southern Penang Pluton, on the other hand, is classified into Batu Maung Granite and Sungai Ara Granite. Figure 1b illustrates the geology map and the study area of USM.

The critical slope of the Lojing area is situated along the Gua Musang-Cameron Highland highway; it covers part of the Western Belt Main Range. The Main Range is generally of the Late Triassic age, majorly consisting of granite (Figure 1c) with several enclaves of metasedimentary rocks [12]. The Main Range Granite is located in the west of the state, stretching along with western Kelantan up to the state boundary of Perak and Pahang. It also serves as the international boundary of Malaysia-Thailand. The geomorphology of the area reveals reserved forests surrounded by mountainous landscapes. Since high topographic landscapes span the region (Figure 1e), it is highly susceptible to slope instabilities. Therefore, data acquisition was performed at the hill-slope topography, spanning along the highway (Figure 1c). The slopes in the study area are unstable due to creeping activities, thus making it an ideal choice for this study. Based on field observation, the surface condition of the slopes is severely disturbed due to ongoing creeping activities. The activities occur at the estimated soil dimensions of 20-m length by 30-m width from the surface. Moreover, broken concrete drainage at the top of the terrace appears due to the instability of the ground motion.

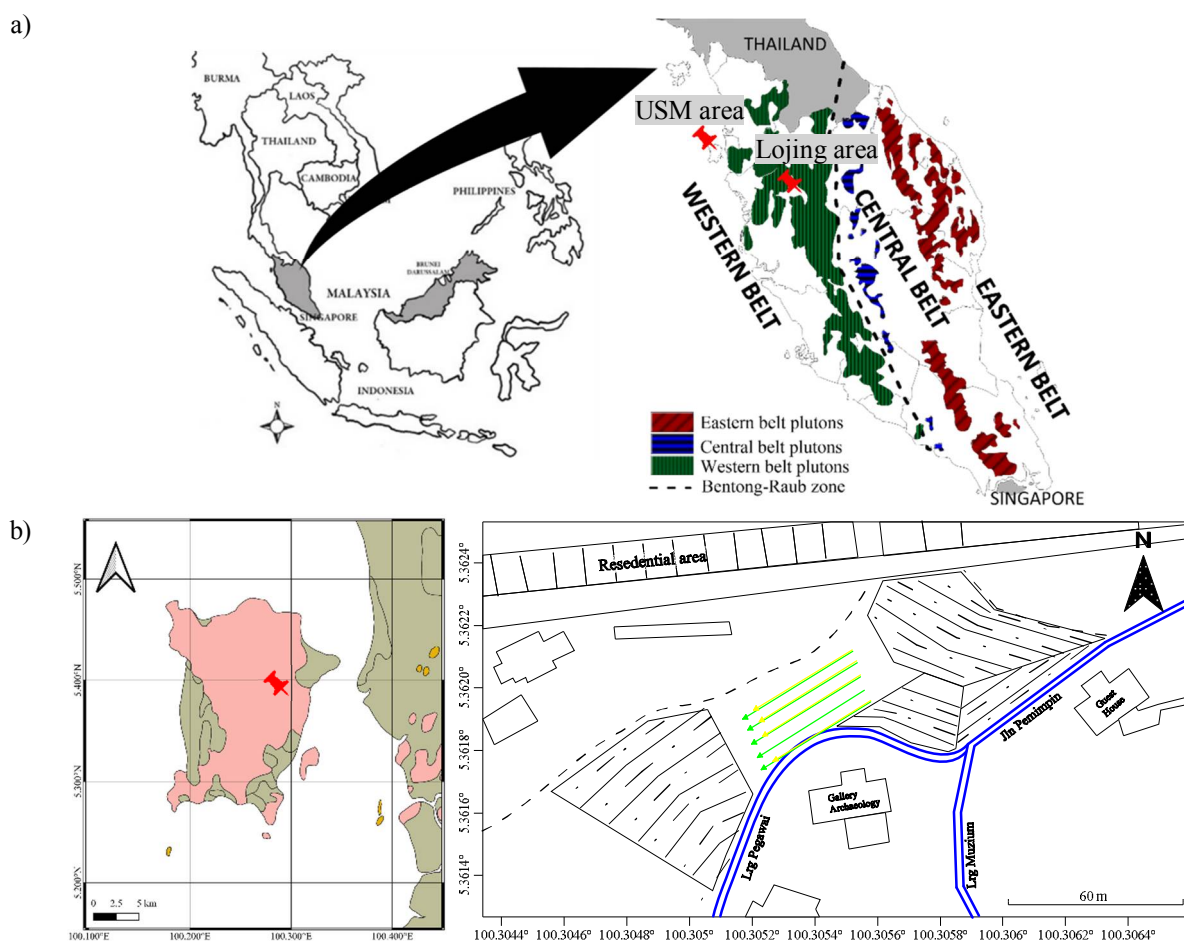


Figure 1. Study areas: (a) Location of the areas and geological setting of Peninsular Malaysia [12]; (b) Geology map of USM [13] and survey area;

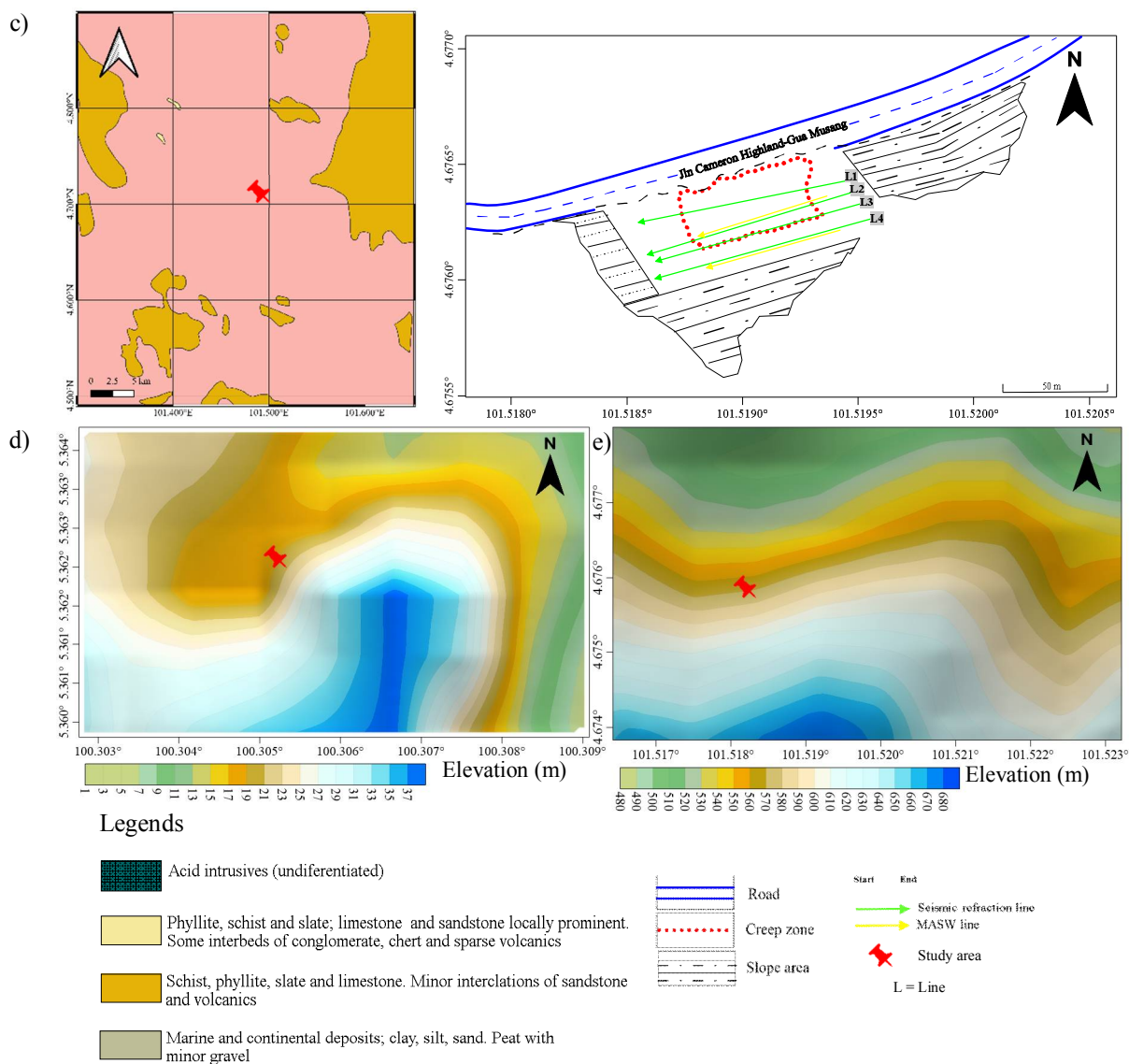


Figure 1 (continued). (c) Geology map of Lojing [13] and survey area; (d) Topography of USM [14]; (e) Topography of Lojing [14]

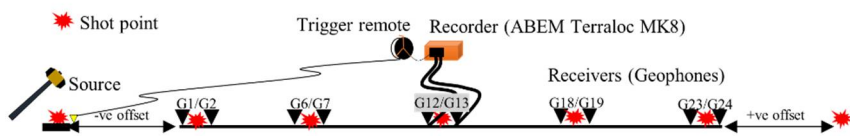
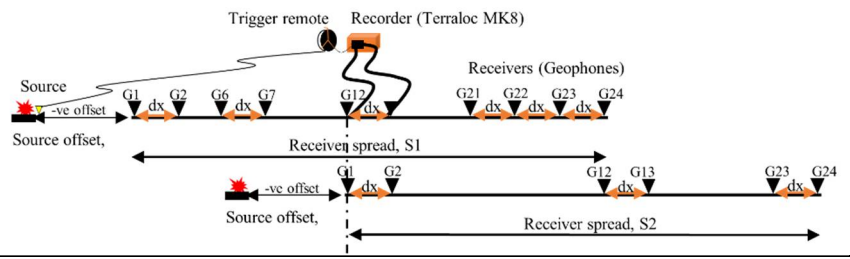
Methodology

Geophysical survey

This survey employs seismic refraction and MASW methods, which constitute three main parts: the source, detector (receiver) and recorder. Both surveying techniques use inline configuration to provide good data correlations. A 5-kg sledgehammer was used as the source of impulsive waves. The wave energy propagated throughout the media and was detected by geophones and recorded by a 24-channel Aktiebolaget Elektrisk Malmletning-Signal Averaging System (ABEM) Terraloc Mark 8 (Mk8) seismograph. A remote trigger geophone triggers the seismograph as soon as the sledgehammer hit a steel striker plate. The seismic refraction technique uses seven-shot points to acquire detailed velocity distributions. Five of these points are inline and the remaining are positive and negative offsets (Table 1). Different geophone spacings were applied based on site constraints and the extension of the failure boundaries. Otherwise, the MASW survey was conducted using low-frequency geophones of 4.5 Hz. This research focuses on the active

acquisition where 24 geophones (detectors) were lined up at a constant spacing (dx) and connected with the seismic cable. The roll-along technique (Table 1) was applied by moving the half-spread of the geophones forward. The half-spread needs to move at least four times to provide four different inline mid-points (in the middle of the receiver spread) in the survey lines. Finally, two-shot points were used at two different negative offset distances. Table 1 shows the survey parameters of seismic refraction and MASW of this research.

Table 1. Survey parameters of seismic refraction and MASW

Seismic Refraction Survey Parameters		
		
Study area	USM	Lojing
No. of line	Five (US1-US5)	Four (LS1-LS4)
Total length	46 m	115 m
Geophone spacing	2 m	5 m
MASW Survey Parameters		
		
Study area	USM	Lojing
No. of line	Five (UM1-UM5)	Two (LM2, LM4)
Total length	23 m x 4 spread (S)	23 m x 4 spread
Geophone spacing	1 m	1 m
Mid-point with spread (S)	0 m (S1), 12 m (S2), 24 m (S3), 36 m (S4)	32 m (S1), 44 m (S2), 56 m (S3), 68 m (S4)

In this seismic refraction survey the data were analysed using Firstpik software [15] for velocity and SeisOpt@2D software [16] used to derive the velocity distribution of the subsurface. Essentially, an accurate picking method ensures the reliability of the velocity model produced. In general SeisOpt@2D operates using a nonlinear optimisation technique known as adaptive simulated annealing, which involves forward modelling [17]. The calculated travel time was then compared with the observed data and the errors between them were optimised, thus generating velocity models with minimum travel time errors. MASW operates based on the dispersive properties of surface waves in a vertically heterogeneous medium. The analysis extracts a dispersion curve from the acquired time series of the Rayleigh waves. The required fundamental mode of the Rayleigh wave dispersion curve was extracted using the Picking tool of the software. It was later re-processed in the DINVER program to generate V_s profile [18]. Inversion analysis produces a shear wave velocity profile from Neighbourhood algorithm computations.

Geotechnical properties

The body wave components can be directly related to the medium of wave propagation's elastic moduli. The most commonly used moduli to characterise soil are the small strain shear

modulus, G_0 , and Young's modulus, E . Both moduli provide the measurement of the material's stiffness. Here, stiffness is the ratio of stress to resulting strain along an axis resulting from shear (G_0) or loading (E) [19, 20]. Essentially, it describes the ability of the material to resist shearing (i.e. change of shape without change of volume). Thus, the shear modulus is equal to the ratio of shear stress to shear strain while Young's modulus, E , is referred to as the compressibility behaviour. Equations (1) and (2) (Table 2) show the relationship of Shear modulus, G_0 , and Young's modulus, E , with ρ as the density of the material. The bulk density, ρ , refers to the measurement of the total amount of solid and water per unit volume [21] and is expressed with Equation (3). Another commonly used parameter in slope stability analysis is the Poisson's ratio, ν [22, 23], which relates the stress field in the slope and the degree of saturation of the soil material [24]. Compared to the shear and Young's moduli, the density estimation does not require the calculation of ν . Thus, it eliminates the potential uncertainties arising from an assumed density. Table 2 shows the summary of the equations used in this work for calculating the elastic moduli.

Table 2. Types of elastic moduli

Elastic modulus	Equation used	References
Shear modulus, G_0	$G_0 = \rho V_s^2$ (1) where V_s = S-wave velocity ρ = density	[19, 20]
Young modulus, E	$E = \frac{\rho V_s^2 (3V_p^2 - 4V_s^2)}{(V_p^2 - V_s^2)}$ (2) where V_s = S-wave velocity V_p = P-wave velocity ρ = density	[19, 20]
	$\rho = \frac{Z}{g}$ (3) where $g = 9.81$ m/s	[21]
	$\gamma = \gamma_0 + 0.002V_p$ (4)	$\gamma_0 = 16$ (loose sand, silt, clay) $\gamma_0 = 17$ (dense sand and gravel) $\gamma_0 = 18$ (mudstone, limestone, conglomerate) $\gamma_0 = 20$ (cracked sandstone, tuff, schist) $\gamma_0 = 24$ (hard rock)
Poisson's ratio, ν	$\nu = \frac{V_p^2 - 2V_s^2}{2(V_p^2 - V_s^2)}$ (5) where V_s = S-wave velocity V_p = P-wave velocity	[22, 23]

The soil competence scale includes the material index, concentration index, stress ratio and density gradient. The material index, M_i , refers to the degree to which the material's modulus of elasticity varies [25]. Also, M_i measures the competency level of the material and it depends on the mineralogical composition of and the physical environment affecting the soil or rock [1]. Equation (6) (Table 3) displays the expression of M_i expressed in terms of elastic modulus, where ν refers to the Poisson's ratio. The concentration index, C_i , is the velocity square ratio as shown in Equation (7). The index shows the compaction status of the soil which depends on both the elastic moduli and the pressure distribution with depths [1]. The stress ratio, S_i , refers to the pressure state where the soil is in a condition of zero horizontal and vertical strains [26]. Essentially, S_i is expressed in terms of ν as given by Equation (8). In general S_i tends to be higher for finer soil compared to coarser soil and is high in loose and cohesionless soil. The density gradient, D_i , represents an increase in bulk density under tectonic stress [1] and is related to the degree of consolidation settlement [27]. Equation (9) displays the expression of D_i , and its calculation requires the value of V_p and V_s . Table 3 shows a summary of equations for the determination of the competence scale.

Table 3. Types of competence scale

Competence scale	Equation used		References
Material index, M_i	$M_i = 1 - 4\nu$	(6)	where ν = Poisson's ratio [25, 28]
Concentration index, C_i	$C_i = \frac{(3-4\alpha)}{(1-2\alpha)}$	(7)	where α refer to velocity square ratio, $\left(\frac{V_s}{V_p}\right)^2$ [25, 29]
Stress ratio, S_i	$S_i = \frac{\nu}{1-\nu}$	(8)	where ν = Poisson's ratio [27, 29]
Density gradient, D_i	$D_i = \left[V_p^2 - \frac{4}{3}V_s^2\right]^{-1}$	(9)	where V_s = S-wave velocity V_p = P-wave velocity [25, 27]

The zonation map of the study area was visualised based on the elastic moduli and competence scale measurement of the soil. The map displays the spatial distribution of potential hazards. The mid-point of the S-wave was used as a reference to generate the integrated analysis using the established equations given in Tables 2 and 3. The data were thoroughly analysed and a contour map was generated using Surfer software. The zonation map is represented by various geo-seismic layers and is based on the initial interpretation of the velocity distribution of P- and S-waves.

RESULTS AND DISCUSSION

Geophysical Parameters

In the presentation of the seismic refraction and MASW data for the USM area using the line sequences of US1&UM1-US5&UM5, these lines follow the slope geometry since US1&UM1 are located at the crest, moving downward to the toe of the slope (US5&UM5). Figure 2 presents the seismic refraction (US1-US5) and 1-D MASW (UM1-UM5) profiles of the area. The locations of the S-wave velocity mid-points are shown in the seismic refraction profiles and marked as S1-S4. The range of P-wave velocity (V_p) for all seismic refraction profiles is 300-3200 m/s. For 1-D MASW profiles, the S-wave velocity (V_s) ranges between 180-500 m/s. The investigation depths for both P-wave and S-wave velocities are 15 m and 20 m respectively. In the US1 profile the P-wave velocity distribution covers the range of 300-1600 m/s, with a gradual velocity increment. Such a velocity increment happens because of the increase in material stiffness, as the S-wave velocity (UM1) shows a gradual increase in the depth of investigation.

This work also studies the two-layer cases for the US1 profile. The 1st layer rests at a depth of <5 m and the corresponding P-wave and S-wave velocities are $V_p = 300-800$ m/s and $V_s = 200-280$ m/s respectively. In the 1st layer the velocities indicate the presence of loose sand from the residual soils. The 2nd layer lies at a depth of >5 m and the corresponding wave velocities are $V_p > 1000$ m/s and $V_s = 280-380$ m/s. Thus, such velocity values may indicate the presence of dense or saturated sand from the residual soils. On the other hand, the 1-D MASW profile has an investigation depth of up to 20 m with high S-wave velocity, i.e. $V_s = 380-430$ m/s. Such a high V_s value may suggest the presence of hardened materials or cohesive soil. The result shows a good correlation with the previous study [30], stating that the velocity of V_s is greater than 380 m/s. Such an observation indicates the existence of hard silt at a depth of >20 m [30].

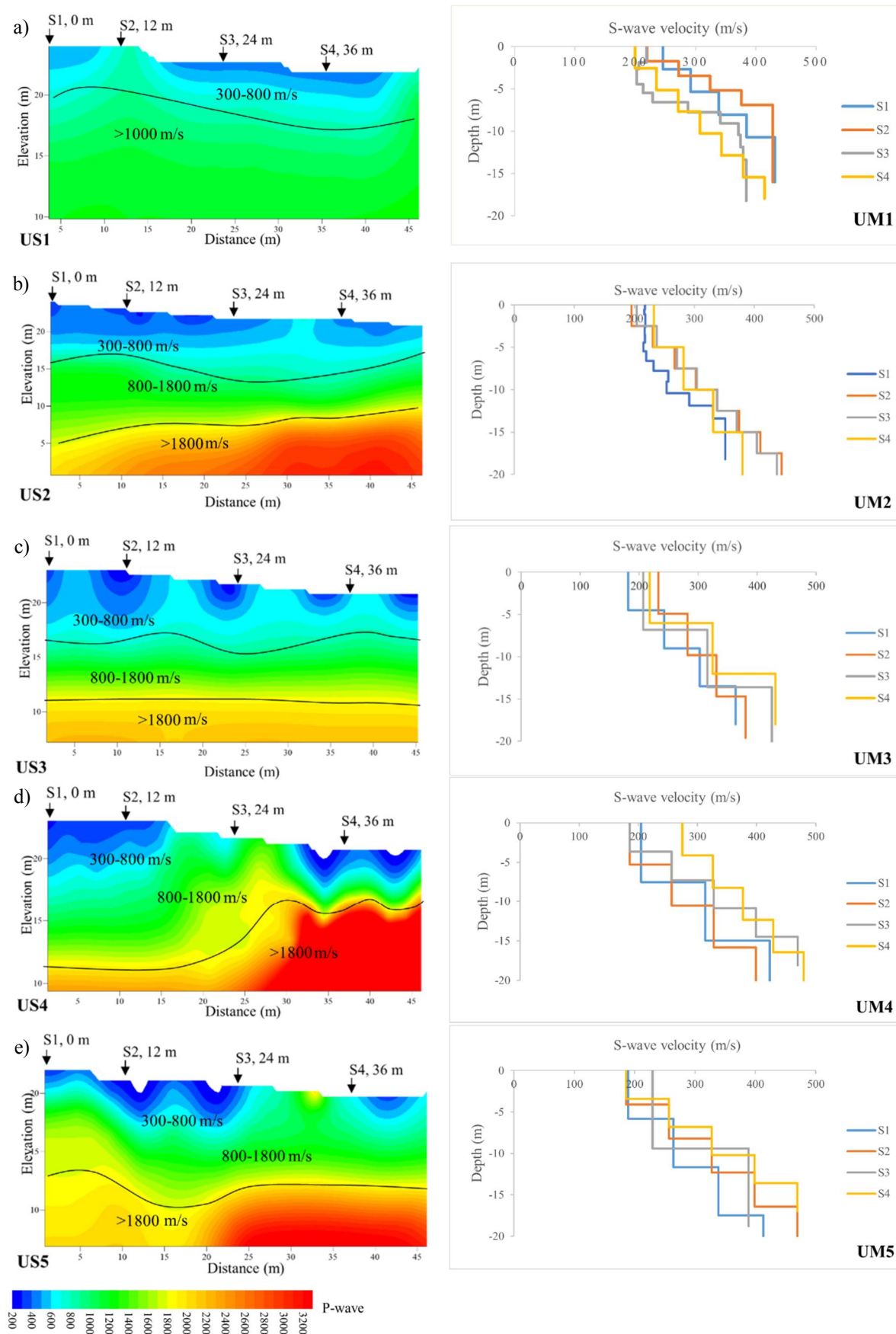


Figure 2. Seismic refraction models and 1-D MASW profiles of the USM area: (a) US1&UM1; (b) US2&UM2; (c) US3&UM3; (d) US4&UM4; (e) US5&UM5

In the US2&UM2 profile (Figure 2b) the velocity distribution shifts toward higher values compared to the previous line profiles. Note that the profile is slightly lower than the US1&UM1 line, which indicates that the depth is marginally deeper. In the US2 profile the P-wave velocity (V_p) covers the range of 300-3200 m/s at a depth of up to 24 m, while in the 1-D MASW of UM1 profile the S-wave velocity (V_s) ranges between 180-450 m/s at a depth of 20 m. The profile indicates three main layers of velocity, which corresponds to the three types of geo-material with possibly different characteristics. The profile also displays the three distinct zones with $V_p=300-800$ m/s at depths of <5 m, representing the topsoil of the study area. With $V_p=800-1800$ m/s at depths of <10 m, it indicates the presence of cohesive material (sandy silt). Alternatively, $V_p>1800$ m/s suggests the presence of firm material or moderately weathered rock of the subsurface. Such an interpretation is consistent with the previous work conducted by Abu Samah et al. [31] in 2016, which revealed the presence of cohesive soil in the USM area with V_p ranges of 808-1483 m/s and 1735-2974 m/s for very stiff and hard soils respectively. The result proves the stability of the profile with the higher measured velocity.

In the seismic refraction models a solid black line indicates the layer profiles. Also, it is plausible to classify the 1-D S-wave model generated from the MASW survey into three subsurface layers. The 1st layer with the velocity of $V_s=180-240$ m/s at a depth of <5 m predominantly represents the topsoil with unconsolidated material. The 2nd layer at a depth of <10 m with a velocity of $V_s=250-340$ m/s represents cohesive materials (sandy silt) in the subsurface. Meanwhile, the 3rd layer of the profile with $V_s=350-460$ m/s at a depth of >10 m indicates hard material/moderate weathered rock. For the US3-US5 and UM3-UM5 profiles (Figures 2c-2e), the distribution of P-wave and S-wave velocities display the same trend as the US2&UM2 profile. In the US4 profile the P-wave velocity (>1800 m/s) and S-wave velocity (280-480 m/s) increase towards the end of the profile line (30-46 m). The UM4 and UM5 profiles indicate a slight difference in the S-wave velocity pattern at a distance of 30-46 m (S4) compared to other velocity profiles (S1-S3). Also, UM4 and UM5 exhibit higher velocity ranges, i.e. $V_s=280-480$ m/s and $V_s=200-480$ m/s respectively. Here, S4 has a slightly higher S-wave velocity in the UM4 and UM5 profiles, which indicates the presence of hard materials.

Figure 3 shows the 2-D seismic refraction models of LS1-LS4 for the Lojing area. Here, V_p ranges between 300-2800 m/s and the investigation depth is about 30 m. The results present the three main layers of velocities, which correspond to the three types of geo-materials with possible different characteristics. The 1st layer indicates $V_p=400-600$ m/s with a depth of <6 m from the surface. Also, V_p increases with the penetration depth of up to 20 m. Next, the 2nd layer exhibits $V_p=800-1400$ m/s. The 3rd layer is at depth >20 m, with a velocity of $V_p>2000$ m/s. In this study the velocity profiles of the Lojing area show heterogeneous subsurface models of the creep zones. The LS4 profile shows the upper condition of the creep zones followed by LS3-LS1. Most importantly, $V_p=400-600$ m/s represents the materials' loose soil and $V_p=800-1400$ m/s represents the highly weathered materials. The trends are continuous for LS4-LS1 (Figures 3a-3d) with hard materials/bedrock identified at depth >20 m with a velocity of $V_p >2000$ m/s. Such an observation implies that the material is a weathered granite.

Figure 3 presents the 1-D MASW profiles of LM4&LM2, which are in line with seismic refraction profiles of LS4&LS2 for the Lojing area. Here, $V_s=150-500$ m/s with depth up to 30 m, and the range comprises three categories, which correspond to three subsurface layers. The 1st layer with $V_s=150-200$ m/s at the depth of <5 m may represent the topsoil with unconsolidated material of loose sand or gravel. The 2nd layer with $V_s=200-400$ m/s at the depth of 5-10 m indicates a stiff

soil profile, representing the extent of unconsolidated material, which is probably the loose sand. The layer indicates the weak zones of the profile, which is where creep zones occur. The 3rd layer ($V_s > 400$ m/s at depth > 10 m) indicates the profiles' weathered layer. For the LS4&LM4 profile (Figure 3a), the high velocities of $V_p (> 1200$ m/s) and $V_s (> 400$ m/s) indicate the weathered bedrock at a depth of > 15 m. Meanwhile, in LS2&LM2 profiles (Figure 3b) the weathered layers are at a depth of < 10 m, where velocities range from 600-800 m/s and 200-350 m/s for V_p and V_s respectively. The presence of unconsolidated material at the depth of < 5 m is the preliminary indicator for the instability of the profiles, plus the observation that the profile is highly weathered due to the lower seismic velocities of P- and S-wave distributions.

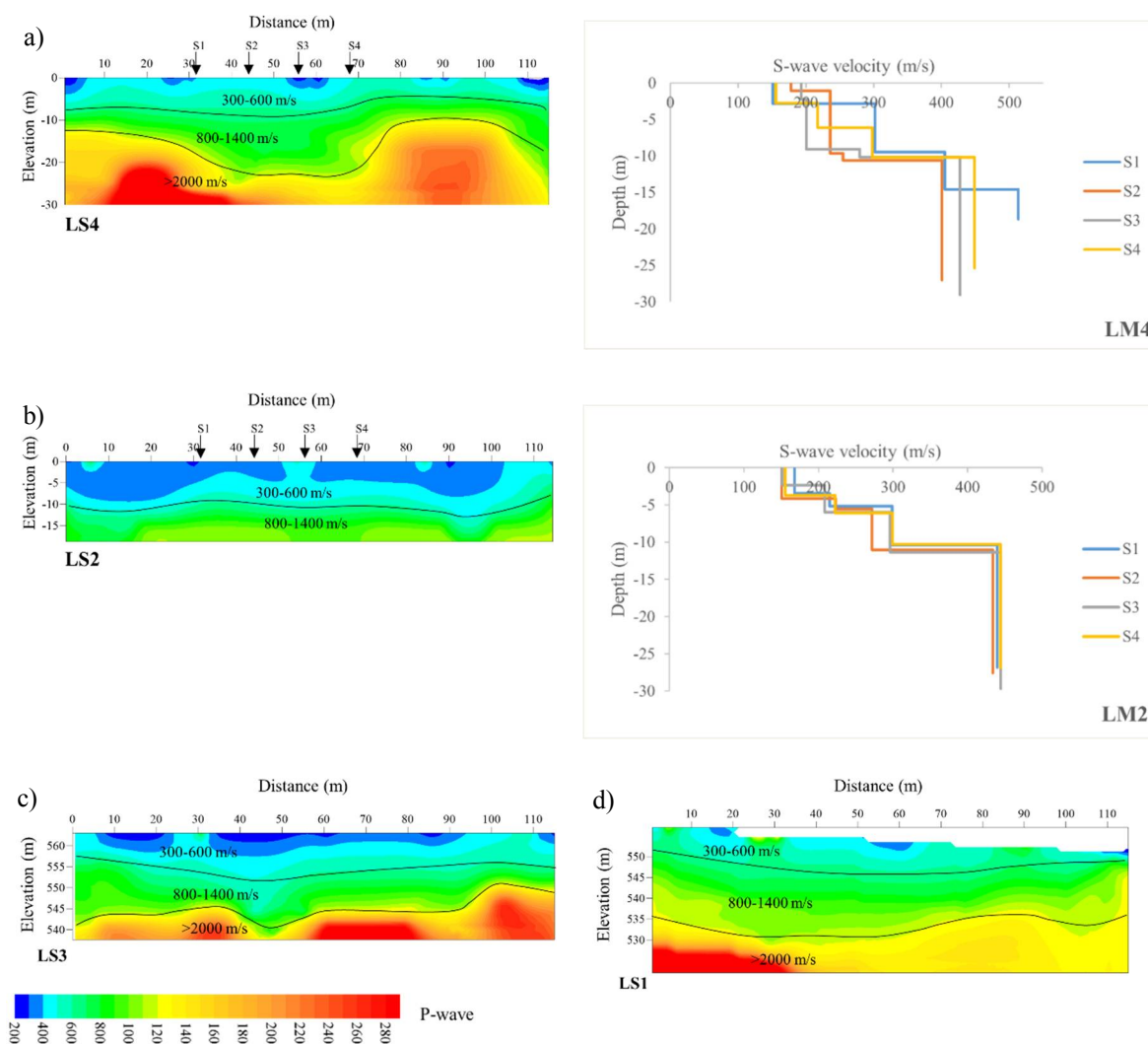


Figure 3. Seismic refraction models and 1-D MASW profiles of Lojing area: (a) LS4&LM4; (b) LS2& LM2; (c) LS3; d) LS1

Geotechnical Parameters

The geotechnical parameters such as the dynamic elastic moduli and the competence scale were derived based on the P- and S-wave velocities. Tables 4 and 5 present the results for both the USM and Lojing areas. According to Akhter et al. [32], there is a direct relationship between the seismic velocity and density. Higher velocity values indicate a higher density with a substantial

degree of soil/rock compaction. In this study the USM study area shows higher dominant density values for three different layers. Comparatively, the Lojing area has a mean density of 1.75-2.06 g/cm³. The density ρ shows an increasing trend with depth, which implies an increase of soil compaction. The Poisson's ratio ν in the USM area displays a broader range, i.e. $\nu = 0.11-0.5$. Here, $\nu=0.5$ indicates an incompressible fluid, whereas ν approaching 0.5 indicates the fully saturated clay. Finally, partially saturated silt or clay has a lower ν value between 0.2-0.4 [26]. The value of ν in the Lojing area shows a non-constant trend. From the 1st to the 2nd layer, the mean ν is between 0.4 - 0.37. In the 3rd layer ν increases to the value of 0.41. The inconstant ν values confirm that the higher ν material is overlain by the lower ν one. In this study the threshold value of ν is 0.4, where $\nu>0.4$ indicates saturated sand. Otherwise, $\nu<0.4$ signifies partially saturated sand or silt [23].

Table 4. Geotechnical parameters of USM study area

Parameter	Geoseismic layer (USM)								
	First layer			Second layer			Third layer		
	Min.	Max.	Mean	Min.	Max.	Mean	Min.	Max.	Mean
Density, ρ (g/cm ³)	1.69	1.95	1.75	1.75	2.87	1.88	1.82	3.00	2.06
Poisson's ratio, ν	0.11	0.49	0.37	0.23	0.50	0.45	0.27	0.50	0.47
Shear modulus (Pa), G_0	5.61E+07	2.17E+08	8.68E+07	6.29E+07	6.13E+08	1.57E+08	1.08E+08	3.46E+09	3.50E+08
Young Modulus (Pa), E	2.68E+07	5.00E+08	2.22E+08	3.28E+07	1.67E+09	4.36E+08	4.85E+07	9.18E+09	9.38E+08
Material index, M_i	-0.96	0.57	-0.47	-0.99	0.10	-0.80	-0.99	-0.07	-0.89
Concentration index, C_i	3.04	10.30	4.09	3.01	5.44	3.25	3.01	4.74	3.13
Stress ratio, S_i	0.12	0.96	0.61	0.29	0.99	0.83	0.37	0.99	0.90
Density gradient, D_i	4.05E-07	2.43E-05	6.04E-06	2.71E-08	4.81E-06	1.23E-06	2.21E-08	1.33E-06	3.59E-07

Table 5. Geotechnical parameters of Lojing study area

Parameter	Geoseismic layer (Lojing)								
	First layer			Second layer			Third layer		
	Min.	Max.	Mean	Min.	Max.	Mean	Min.	Max.	Mean
Density, ρ (g/cm ³)	1.70	1.74	1.72	1.72	1.79	1.75	1.75	1.99	1.83
Poisson's ratio, ν	0.33	0.45	0.40	0.31	0.45	0.37	0.31	0.47	0.41
Shear modulus (Pa), G_0	3.25E+07	7.55E+07	5.47E+07	6.78E+07	2.22E+08	1.10E+08	1.23E+08	4.95E+08	2.37E+08
Young Modulus (Pa), E	9.29E+07	2.61E+08	1.60E+08	1.93E+08	5.95E+08	3.08E+08	3.61E+08	1.38E+09	6.90E+08
Material index, M_i	-0.78	-0.31	-0.61	-0.80	-0.23	-0.48	-0.87	-0.23	-0.65
Concentration index, C_i	3.24	4.06	3.50	3.23	4.26	3.74	3.13	4.26	3.44
Stress ratio, S_i	0.49	0.80	0.68	0.44	0.81	0.60	0.44	0.88	0.71
Density gradient, D_i	3.93E-06	1.16E-05	6.85E-06	2.14E-06	8.54E-06	4.74E-06	3.51E-07	4.53E-06	1.58E-06

Other implemented elastic parameters are the shear modulus (G_0) and Young modulus (E). The USM area exhibits higher values of G_0 and E compared to the Lojing area. Such observation reveals that the overburden condition is more stable in the USM area. The competence scale shows the USM study area is more stable than the Lojing area. The 1st layer displays a broader range of material index, i.e. $M_i = -0.96 - 0.57$, which indicates fair to high competence compared to the Lojing area. Also, the 1st layer exhibits $M_i = -0.78 - -0.31$, which represents an incompetent condition. In the USM area the concentration index value C_i for the 1st layer is broader in range and decreases with a range of 3.01-5.44 and 3.01-4.74 for the 2nd and 3rd layers respectively. These ranges imply a fairly competent condition for the overburden [27, 28]. In the Lojing area the value of C_i indicates an incompetent condition with lower range values as compared to the USM area.

A zonation map classifies and visualises the overburden condition of an area; it considers the relation of the seismic velocity to the geotechnical properties. The mid-point location with V_s velocity is integrated to the V_p velocity based on the relation to the geophysical properties. The data are rearranged based on the seismic velocity layer and are presented in Figure 4. Three different parameters are selected and mapped based on the depth condition for different seismic layers as in earlier interpretations. The shear modulus G_θ proportionally increases with depth. For the USM area, the 1st layer has a G_θ value of $<1.4 \times 10^8$ Pa at <5 m depth. The zone is stable compared to the Lojing area, which has a low G_θ (8.0×10^7 Pa). A small G_θ represents unstable soil conditions, which implies weak material competence. Also, G_θ increases with depth, and the USM area shows a broader G_θ range in contrast to the Lojing area. The 3rd layer has a relatively higher G_θ . Here, $G_\theta > 3.0 \times 10^8$ Pa and $G_\theta > 1.5 \times 10^8$ Pa for the USM area and the Lojing area respectively. Recall that the Young modulus E represents the elastic stiffness of the material and note also that Tables 4 and 5 display the definition of E . The USM area shows a higher E for a different layer, which reveals the stability of the soil condition.

The Poisson's ratio ν in the USM study area shows an incompressible condition in the 3rd layer. It also corresponds to the saturated condition with values of $\nu > 0.4$, indicating an increase in the moisture content [33]. In the 1st and 2nd layers of the Lojing area ν dominates with the values < 0.38 , which indicates a fairly to moderately competent condition. The material index M_i addresses the degree of material competence based on their elastic moduli, where the values generally lie at a range of +1 and -1 [1]. The USM area shows a variation of M_i between -1 - 0.5. The 1st layer at a depth of < 5 m has M_i ranging between -0.7 - 0.1. The range increases with increasing depth, where M_i is between -1 and -6 in the 3rd layer at a depth of > 10 m. These conditions reveal that the USM area has less competent material within this depth profile. In the Lojing area the M_i value lies between -0.76 and -0.26, which indicates a dominant incompetent condition. Also, the 1st layer profile (< 5 m) shows a lower value of M_i , i.e. between -0.68 and -0.36. Previous researchers [1, 27] indicated the ranges of $-1 < M_i < -0.5$, $-0.5 < M_i < 0$, $0 < M_i < 0.5$ and $M_i > 0.5$ as incompetent to slightly competent, fairly to moderately competent, competent, and highly competent materials respectively. The USM study area shows a broader range of competent material and it has a more stable condition than the Lojing area. In general the Lojing area has a value of M_i ranging from -0.7 to -0.4, which indicates incompetent materials. Figure 4 shows the zonation maps of the USM and Lojing area.

Table 6 shows a summary of the direct shear test results for both study areas. In the USM area three undisturbed soil test samples were collected using a hand auger at a depth interval of 1.0 m. From the results, the values of effective friction angle ϕ' are subtle for the depth range of 1-3 m. Such an observation indicates the same soil material, but as the depth increases to 3.0 m, the values of ϕ' increase slightly. It is clear that the material at this depth is cohesive or dense (sandy silt), which tends to promote slope failure compared to low values of ϕ' that represent less cohesive or loose material. The residual soil shear strength parameters are highly inconsistent, and they increase in strength with increasing depth [34, 35]. The higher values of ϕ' shows a slope whose condition is considered to be stable.

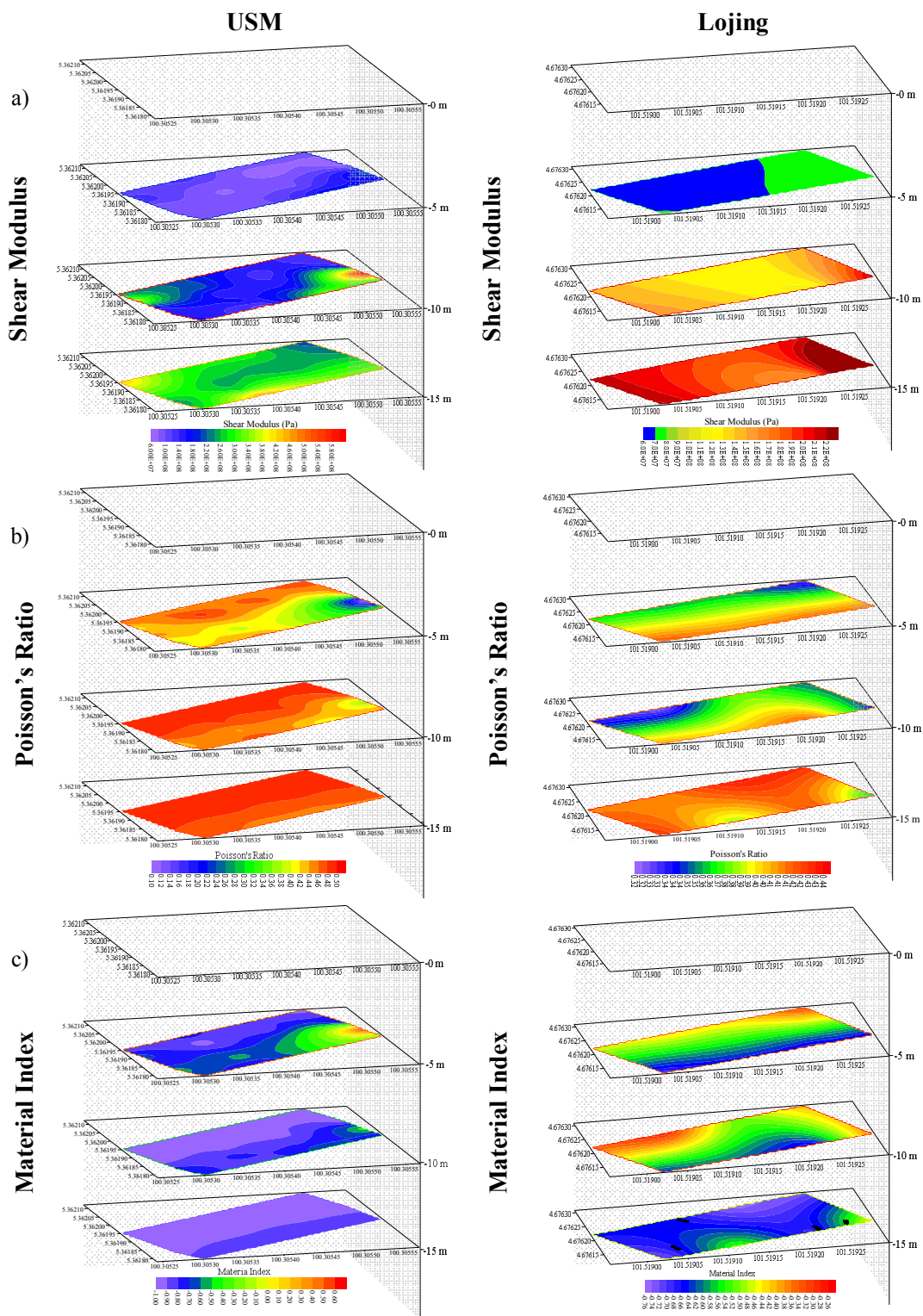


Figure 4. Zonation maps of USM and Lojing area: (a) Shear modulus; (b) Poisson’s ratio; (c) Material index

At the Lojing area, ϕ' ranges between $27.3-47.3^\circ$, and the effective cohesion c' ranges between 9.58-29.9 kPa. Such a high value of c' implies a critical slope condition. In contrast, the USM archaeology area (a stable slope) has lower values of shear strength parameters. The reason is that at the Lojing area (a critical slope) the soil sample was taken at a slightly stronger soil area,

which gives the difference in the value range. In addition, the soil type in Lojing is gravel silt, which gives high values of shear strength parameters. From the results, the shear strength parameters decrease with increasing depth, and ϕ' is from 43.3° to 27.3° , which indicates an unstable condition of soil materials.

Table 6. Summary of results of shear box test for USM and Lojing area

Shear strength parameter of USM				
c' (kPa)	tan ϕ'	ϕ' (degree)	Depth (m)	Soil type
29	0.441	23.8	1	sandy SILT
5	0.385	21.0	2	sandy SILT
-13	0.55	28.8	3	sandy SILT
Shear strength parameter of Lojing				
c' (kPa)	tan ϕ'	ϕ' (degree)	Depth (m)	Soil type
9.58	0.9743	43.3	0.5	gravel SILT
29.9	0.5174	27.3	1	gravel SILT

CONCLUSIONS

The zonation maps present the site classification of the study areas. The maps indicate that the USM area has more competent soil deposit compared to the Lojing area. The results clarify the site conditions, facilitate seismic hazard assessment, and ascertain the rank of site, revealing the competency of the subsurface material. The integrated geophysical method with supported data from the geotechnical analysis help to understand the behaviours of the slope properties. The geotechnical parameters form a vast improvement of the standard discrete sampling/testing of site investigations, where a large volume is often characterised by very sparse data. The main benefit of this study is to provide spatial information relating to the saturation state and potential strength of the ground. This information is crucial for an accurate definition of ground models.

ACKNOWLEDGEMENTS

The authors thank the Ministry of Higher Education Malaysia which provided the Fundamental Research Grant Scheme (project code FRGS/1/2/2018/STG09/USM/03/2) for work entitled “Development of 2-D linear inversion algorithm from geophysical approach for soil or rock characteristics”. They also thank USM which provided Research University Grant (1001/PFIZIK/8011110) for work entitled “Integrated geophysical characterisation of geothermal exploration and strategy for sustainable use of geothermal resources.”

REFERENCES

1. K. Abdelrahman, E. Ibrahim, S. Qaysi, S. Mogren, F. Zaidi and H. Ghrefat, “Evaluation of kinetic moduli and soil competence scale of soil profiles in Jizan area, southwestern Saudi Arabia”, *Arab. J. Geosci.*, **2021**, *14*, Art.no.172.
2. R. E. S. Fat-Helbary, K. O. El-Faragawy and A. Hamed, “Soil geotechnical characteristics for seismic risk mitigation at the southern extension of Marsa Alam city, Egypt”, *NRIAG J. Astron. Geophys.*, **2019**, *8*, 1-14.
3. S. Morelli, S. Utili, V. Pazzi, R. Castellanza and X. Fan, “Landslides and geophysical investigations: Advantages and limitations”, *Int. J. Geophys.*, **2019**, *2019*, Art.no.8732830.

4. B. G. Chae, H. J. Park, F. Catani, A. Simoni and M. Berti, "Landslide prediction, monitoring and early warning: A concise review of state-of-the-art", *Geosci. J.*, **2017**, *21*, 1033-1070.
5. H. Almalki, A. K. El-Werr and K. Abdel-Rahman, "Estimation of near-surface geotechnical parameters using seismic measurements at the proposed KACST expansion site, Riyadh, KSA", *Arab. J. Geosci.*, **2011**, *4*, 1131-1150.
6. S. Yilmaz and Z. Kamaci, "Resistivity and seismic refraction studies on kısıklı landslide (Antalya, Turkey)", *Int. J. Comput. Exp. Sci. Eng.*, **2018**, *4*, 9-14.
7. L. W. Abramson, T. S. Lee, S. Sharma and G. M. Boyce, "Slope Stability and Stabilization Methods", 2nd Edn., John Wiley and Sons Inc., New York, **2002**, pp.1-102.
8. G. C. Anukwu, A. E. Khalil and K. B. Abdullah, "Evaluating the effectiveness of the MASW technique in a geologically complex terrain", *J. Phys. Conf. Ser.*, **2018**, *995*, Art.no.012059.
9. B. Mi, J. Xia, C. Shen, L. Wang, Y. Hu and F. Cheng, "Horizontal resolution of multichannel analysis of surface waves", *Geophys.*, **2017**, *82*, 51-66.
10. A. E. Khalil, M. Nawawi, M. H. Arifin, F. M. Abdullah, J. S. Kayode, N. Usman and Arisona, "Soil investigation at wet world hot spring complex for future development using active multichannel analysis of surface waves", *Sains Malays.*, **2017**, *46*, 537-543.
11. W. S. Ong, "The Geology and Engineering Geology of Pulau Pinang", Jabatan Penyiasatan Kajibumi Malaysia, Kuala Lumpur, **1993**, pp.1-74.
12. J. K. Raj, "Geomorphology", in "Geology of Peninsular Malaysia" (Ed. C. S. Hutchison and D. N. K. Tan), Geological Society of Malaysia, Kuala Lumpur, **2009**, Ch.2.
13. R. B. Tate, D. N. K. Tan and T. F. Ng, "Geological map of Peninsular Malaysia", in "Geology of Peninsular Malaysia" (Ed. C. S. Hutchison and D. N. K. Tan), Geological Society of Malaysia, Kuala Lumpur, **2009**.
14. Google Earth, "Topography of Lojing and USM area", **2021**, <https://earth.google.com> (Accessed: August 2021).
15. Interpex Software, "Firstpix (Version 4.21) [Computer software]", Seismic refraction software tools, **1998**, http://www.interpex.com/dos_programs/refrac.htm#FIRSTPIX.
16. Optim Software, "SeisOpt@2D (Version 3.5) [Computer software]", Software and data solutions, **2003**, <https://optimsoftware.com/>.
17. M. Amirabdollahian and B. Datta, "Application of simulated annealing and adaptive simulated annealing in search for efficient optimal solutions of a groundwater contamination related problem", in "Computational Optimization in Engineering-Paradigms and Applications" (Ed. H. Peyvandi), Intech Open, London, **2017**, Ch.7.
18. M. Wathelet, "An improved neighborhood algorithm: Parameter conditions and dynamic scaling", *Geophys. Res. Lett.*, **2008**, *35*, Art.no.L09301.
19. C. R. I. Clayton, "Stiffness at small strain: Research and practice", *Géotech.*, **2011**, *61*, 5-37.
20. G. Mavko, T. Mukerji and J. Dvorkin, "The Rock Physics Handbook", 3rd Edn., Cambridge University Press, Cambridge, **2020**, pp.112-114.
21. S. S. Tezcan, A. Keceli and Z. Ozdemir, "Allowable bearing capacity of shallow foundations based on shear wave velocity", *Geotech. Geol. Eng.*, **2006**, *24*, 203-218.
22. A. N. Salleh, N. M. Muztaza, R. Sa'ad, M. T. Zakaria, N. Mahmud, F. N. Rosli and N. Samsudin, "Application of geophysical methods to evaluate soil dynamic properties in Penang Island, Malaysia", *J. Asian Earth Sci.*, **2021**, *207*, Art.no.104659.

23. S. Uhlemann, S. Hagedorn, B. Dashwood, H. Maurer, D. Gunn, T. Dijkstra and J. Chambers, “Landslide characterization using P–and S–wave seismic refraction tomography—the importance of elastic moduli”, *J. Appl. Geophys.*, **2016**, 134, 64-76.
24. A. B. Huang, J. T. Lee, Y. T. Ho, Y. F. Chiu and S. Y. Cheng, “Stability monitoring of rainfall-induced deep landslides through pore pressure profile measurements”, *Soils Found.*, **2012**, 52, 737-747.
25. S. Shebl, K. S. Gemail, M. Attwa, S. A. Soliman, A. Azab and M. H. Farag, “Utilizing shallow seismic refraction in defining the geotechnical properties of the foundation materials: A case study at New Minia city, Nile valley, Egypt”, *Egypt. J. Pet.*, **2019**, 28, 145-154.
26. J. E. Bowles, “Foundation Analysis and Design”, 5th Edn., McGraw-Hill, Berkshire, **1996**, pp.589-592.
27. A. M. Abudeif, A. E. Raef, A. A. Moneim, M. A. Mohammed and A. F. Farrag, “Dynamic geotechnical properties evaluation of a candidate nuclear power plant site (NPP): P-and S-waves seismic refraction technique, northwestern coast, Egypt”, *Soil Dyn. Earthq. Eng.*, **2017**, 99, 124-136.
28. M. H. Khalil and S. M. Hanafy, “Geotechnical parameters from seismic measurements: Two field examples from Egypt and Saudi Arabia”, *J. Environ. Eng. Geophys.*, **2016**, 21, 13-28.
29. F. K. Ghanem, H. Al Amoush and E. Al-Tarazi, “Geotechnical engineering evaluation of superficial deposits utilizing seismic methods at Al al-Bayt University, Jordan”, *Iraqi Geol. J.*, **2021**, 54, 11-28.
30. S. N. M. A. Tan, M. E. Tonnizam, R. Saad, M. F. Md Dan, M. M. Nordiana, Z. A. M. Hazreek and A. Madun, “Correlation of resistivity value with geotechnical n-value of sedimentary area in Nusajaya, Johor, Malaysia”, *J. Phys. Conf. Ser.*, **2018**, 995, Art.no.012079.
31. R. Nadia, R. Saad, N. Muztaza, N. A. Ismail and M. M. Saidin, “Geotechnical parameters study using seismic refraction tomography”, *J. Teknol.*, **2016**, 78, 93-98.
32. G. Akhter, Y. Khan, A. A. Bangash, F. Shahzad and Y. Hussain, “Petrophysical relationship for density prediction using Vp & Vs in Meyal oilfield, Potwar sub-basin, Pakistan”, *Geod. Geodyn.*, **2018**, 9, 151-155.
33. S. Pasquet, L. Bodet, A. Dhemaied, A. Mouhri, Q. Vitale, F. Rejiba, N. Flipo and R. Guérin, “Detecting different water table levels in a shallow aquifer with combined P-, surface and SH-wave surveys: Insights from VP/VS or Poisson's ratios”, *J. Appl. Geophys.*, **2015**, 113, 38-50.
34. A. S. A. Rahman, M. J. M. Noor, I. B. M. Jais, N. Sidek and J. Ahmad, “Shear strength of granitic residual soil in saturated and unsaturated conditions”, *AIP Conf. Proc.*, **2018**, 2020, Art.no.020003.
35. D. Jamalludin, F. Ahmad and R. Z. Abidin, “Threshold values of shear strength parameters of soils taken from slope failures and stable slopes in Malaysia”, *Int. J. Latest Res. Sci. Technol.*, **2015**, 3, 10-14.